JOURNAL OF GEOPHYSICAL RESEARCH, VOL. ???, XXXX, DOI:10.1029/,

A Generalized Approach to Estimating Diffusion Length of Stable Water Isotopes from Ice Core Data

Emma C. Kahle,[1] Christian Holme,[2] Tyler R. Jones,[3] Vasileios Gkinis,[2]

and Eric J. Steig,[1]

Corresponding author: Emma C. Kahle, Earth and Space Sciences Department, University of Washington, Seattle, WA, USA. (eckahle@uw.edu)

[1]Department of Earth and Space Sciences,
University of Washington, Seattle,
Washington, USA.

[2]The Niels Bohr Institute, Centre for Ice
and Climate, Juliane Maries Vej 30, 2100
Copenhagen, Denmark

[3]Institute of Arctic and Alpine Research,
University of Colorado, Boulder, CO
80309-0450, USA

Abstract.

Diffusion of water vapor in the porous firn layer of polar ice sheets causes the damping of high-frequency variations in water-isotope ratios. Spectral analysis of water isotope profiles from ice cores to determine characteristic firn-diffusion lengths can provide information about firn conditions in the past. High-resolution water isotope data were obtained by continuous flow analysis (CFA) from ice cores from the West Antarctic Ice Sheet Divide and the South Pole. The spectra of CFA data from these cores show different characteristics than the spectra of data obtained from measurements of discrete ice-core samples. The higher resolution and greater signal to noise ratio of CFA data may bias the estimation of diffusion lengths as obtained from techniques developed for discrete data. Two new diffusion-length estimation techniques are proposed, which apply generally to both CFA and discretely-sampled data. The application of these results to the determination of temperature change and the investigation of firn processes through time are illustrated.

1. Introduction

Water isotope data from ice cores have long been used as climate proxies, based on the temperature-dependent distillation of water isotope ratios (e.g. δ^{18}O) in the atmosphere [*Epstein et al.*, 1951; *Dansgaard*, 1954, 1964]. This traditional method for obtaining past temperature relies on empirical correlations that only approximate the physical processes involved. An alternative approach uses the signal of isotope diffusion preserved in the ice as a proxy for past site temperature [*Johnsen et al.*, 2000].

Water isotope diffusion occurs primarily in the firn layer, snowfall in the upper tens of meters of an ice sheet that has yet to be fully compressed into ice. Because firn is permeable, water molecules can diffuse in the vapor phase, damping the seasonal variations and high-frequency noise of the original isotope signal. Because the diffusion process depends on temperature, a temperature record can be obtained by determining the extent of diffusion that has occurred, quantified as a "diffusion length" [*Johnsen et al.*, 2000]. This method is independent of conventional assumptions about isotope fractionation before deposition, and thus has the potential to improve upon on conventional ice core paleotemperature methods. Diffusion estimates also provide constraints on past firn conditions and ice thinning history.

With these motivations, estimates of diffusion length have been made for ice cores in both Greenland and Antarctica [*Simonsen et al.*, 2011; *Gkinis et al.*, 2014; *van der Wel et al.*, 2015; *Jones et al.*, 2017a; *Holme et al.*, 2017]. Most estimates have used spectral analysis, as originally suggested by *Johnsen* [1977], to determine the degree to which high frequencies in the data have been damped. Existing methods for estimating diffusion do

not work equally well for all data sets. In particular, high-resolution isotope data obtained using recently-developed continuous-flow measurements systems have somewhat different spectral characteristics than those obtained by measurements of discrete ice samples [*Jones et al.*, 2017a], complicating estimation of diffusion lengths. In this paper we describe two general approaches to determining diffusion length. We use new data as well as previously published data to demonstrate the effectiveness of these approaches on all data sets. We also discuss potential sources for these spectral differences in the continuously measured data.

2. Isotope Diffusion Theory

The majority of water isotope diffusion occurs in the firn layer where interconnected air pathways allow water vapor to diffuse vertically through the firn column. After firn densification has sealed off bubbles in the ice, vapor diffusion ceases and solid ice diffusion takes over. The process in solid ice has a diffusivity orders of magnitude smaller than that of vapor diffusion, and we do not consider it in this study.

The isotope profile in the firn layer of an ice sheet changes both due to diffusion across isotopic gradients and due to densification of the firn. These changes to the isotopic profile can be described by Fick's second law, the basic advection-diffusion equation:

$$\frac{\partial \delta}{\partial t} = D\frac{\partial^2 \delta}{\partial z^2} - \dot{\epsilon} z \frac{\partial \delta}{\partial z}, \tag{1}$$

where δ is the isotope ratio, D is the diffusivity coefficient, z is the vertical coordinate assuming an origin fixed on a sinking layer of firn, and $\dot{\epsilon}$ is the vertical strain rate [*Johnsen*, 1977; *Whillans and Grootes*, 1985]. The term $\dot{\epsilon} z$ can be thought of as the vertical velocity.

As shown by *Johnsen* [1977] and subsequently used in many diffusion studies [*Cuffey and Steig*, 1998; *Whillans and Grootes*, 1985; *Johnsen et al.*, 2000; *Simonsen et al.*, 2011; *Gkinis et al.*, 2014; *van der Wel et al.*, 2015; *Jones et al.*, 2017a; *Holme et al.*, 2017], a solution for the isotopic profile at time t and depth z in the firn column is given by:

$$\delta(z,t) = S(t)\frac{1}{\sigma\sqrt{2\pi}}\int_{-\infty}^{\infty}\delta(z,0)\exp\left(\frac{-(z-u)^2}{2\sigma^2}\right)du, \tag{2}$$

where $S(t)$ is the total thinning the layer has experienced due to ice flow from $t = 0$ to $t = t'$:

$$S(t') = \exp\left(\int_0^{t'}\dot{\epsilon}(t)dt\right), \tag{3}$$

and σ is the "diffusion length." The diffusion length quantifies the average vertical displacement of water molecules (excluding the advection) before they reach the bottom of the firn.

Equation 2 is the convolution of the initial isotope profile, $\delta(z,0)$, with a Gaussian filter of standard deviation of the diffusion length σ [*Johnsen et al.*, 2000]:

$$\mathcal{G} = \frac{1}{\sigma\sqrt{2\pi}}\exp\left(\frac{-z^2}{2\sigma^2}\right). \tag{4}$$

To solve this convolution, we take the Fourier transform of both sides of the equation:

$$\delta(z,t) = \delta(z,0) * \mathcal{G} \qquad \Rightarrow \qquad \hat{\delta}(z,t) = \hat{\delta}(z,0)\cdot\hat{\mathcal{G}}, \tag{5}$$

where $*$ represents the convolution and $\hat{}$ represents the Fourier transform. The Fourier transform of a Gaussian remains a Gaussian:

$$\mathfrak{F}(\mathcal{G}) = \hat{\mathcal{G}} = \exp\left(\frac{-k^2\sigma^2}{2}\right), \tag{6}$$

where k is wavenumber. Equation 6 represents the ideal exponential model for diffusion. One can solve for σ by optimizing the fit between Equation 6 and the power spectral

density of the isotope data, which is quite close to this ideal model. Repeating this method over consecutive windowed sections of data yields diffusion length estimates through the length of an ice core.

3. Water Isotope Data

For most ice cores, water isotope data have been measured discretely by melting vertical sections of the core to produce a sample. The isotope ratio of each discrete sample is measured by mass spectrometry or laser spectroscopy [*Kerstel et al.*, 1999; *Lis et al.*, 2008; *Gupta et al.*, 2009; *Brand et al.*, 2009]. More recently, ice core water isotope measurements have been measured on continuous flow analysis (CFA) systems. CFA systems continuously feed the water stable isotopes of the melting core into a laser spectrometer, yielding high resolution data [*Gkinis et al.*, 2011; *Emanuelsson et al.*, 2015; *Jones et al.*, 2017b]. The sample travels in a series of tubing through a filter unit and vaporizer before entering the spectrometer. For more thorough information on the CFA set up used for the data in this paper, see *Jones et al.* [2017b]. Depending on the amount of effort committed, discrete analyses can produce resolutions ranging from $\sim$1/2 meter for entire ice cores to $\sim$1 cm for smaller sections of ice cores. CFA has been used to produce results with an effective resolution of 1/2 cm for an entire ice core record.

In this paper, we use previously-published data from the WAIS Divide ice core (WDC) [*Jones et al.*, 2017b] and new data from an ice core at the South Pole (SPC). Details of the SPC ice core project are given in [*Casey et al.*, 2014]. Both the WDC and SPC ice cores were measured continuously at the Institute of Arctic and Alpine Research (INSTAAR) at the University of Colorado and cross-calibrated by discrete measurements at the University of Washington IsoLab. For WDC, a Picarro L2130-i laser spectrometer

was used for δ^{18}O and δD measurements; details are given in *Jones et al.* [2017b]. For the SPC, we added a Picarro L2140-*i* [*Steig et al.*, 2014] to the CFA system to additionally obtain measurements of δ^{17}O. We use the first 2800 meters of WDC, corresponding to approximately the last 30,000 years. As of this writing, the full SPC record is still being processed; we use two 50-meter sections, one from the early Holocene and one from the last glacial period. For comparison we also use other published discrete and continuous water isotope data sets from Greenland and Antarctic cores presented in *Oerter et al.* [2004]; *Gkinis et al.* [2011]; *Steig et al.* [2013]; *Svensson et al.* [2015]; *Holme et al.* [2017].

To calculate the power spectral density of these data sets, we use Burg's spectral analysis method and assume a μ-order autoregressive process. Figure 1 compares resulting spectra, normalized to unit power spectral density at the lowest frequency. We follow the methods used in *Gkinis et al.* [2014] to minimize the misfit in a least squares sense between the power spectral density of the data and a model given by the following:

$$P_\sigma = P_0 e^{-k^2\sigma^2} \tag{7}$$

where P_0 is the original power level before diffusion. A key assumption made in this process is that any variations in frequency in the power spectrum of the surface snow are small compared to the damping of high frequencies due to diffusion.

Furthermore, the right panel of Figure 1 demonstrates the evolution of CFA measurements through time, which provides insight into how the CFA system affects the power spectrum of the data. These effects arise from improvements to the Picarro instruments and software combined with changes in the CFA melt rate. This result is due to the averaging of raw data to an even depth scale prior to calculation of the spectrum. With

different melt and aquistions rates of the system and of the instrument, the number of raw points averaged over for each even depth affects the smoothness of the resulting data set. Averaging over more data points at each sampled depth produces a smoother data set with further-damped high frequencies. For example, the Dome F core was measured on a Picarro 1102 instrument with a melt rate of about 3cm/sec and instrument aquisition rate of approximately 0.1Hz, resulting in roughly 1-point averages. Software improvements increased the data aquisition rate of the instrument, and the NEEM core data was averaged over roughly 2 to 3 points. The WDC core was measured on a Picarro 2130, with an aquisition rate of about 1.2Hz, and a decreased melt rate of 2.5cm/s, resulting in rougly 14-point averages. The SPC core was measured on a system with very similar specifications as that of the WDC core, but a Picarro 2140 instrument was used, which might have resulted in higher noise level due to increased sensitivity to δ^{18}O measurements. See Table **??** for a complete summary of the measurement of each core. This careful accounting of changes to the CFA and measurement systems through time explains some of the differences seen in the resulting spectra.

4. Previous Methods of Estimating Diffusion Length from Data

Previous methods of estimating diffusion length have been effectively used for discretely-sampled data in a number of studies [*Johnsen et al.*, 2000; *Simonsen et al.*, 2011; *Gkinis et al.*, 2014; *van der Wel et al.*, 2015]. These methods also work well with spectra from theoretically derived synthetic data [*Holme et al.*, 2017]. These methods are based off of the exponential model in Equation 7 and are effective because the spectra of these discretely-sampled and synthetically created data match closely with the exponential model. However, these diffusion estimation methods can not be applied to spectra from

CFA data because these spectra deviate from an exponential model, with power decaying more slowly toward higher frequencies. This deviation occurs in the frequency range of $10-40$ cycles/m or approximately $2.5-10$ cm ice. This type of behavior is referred to as a long memory process and can likely be explained by memory processes within the CFA system. Figure 1 demonstrates this spectral difference between the spectra of discretely- and continuously-measured data.

For both discretely- and continuously-measured data, a number of different approaches have been used to obtain the diffusion length from spectral data fit. To estimate the extent of diffusion that occurred in the firn, each of these methods separates the spectral power added from the measurement process from the firn diffusion signal. The details of how each method separates this measurement noise differentiate the different methods.

One approach to removing the effects of measurement noise from the diffusion signal is to measure differential diffusion, the difference between diffusion lengths of each isotope. This approach avoids the issue of measurement noise because the added noise is the same for each isotope. However, *Holme et al.* [2017] showed that differential diffusion methods are less precise and less accurate when converting to temperature. thus we focus only on the single-isotope diffusion methods in this paper.

A method for estimating diffusion length from a single isotope is given in *Gkinis et al.* [2014], which mathematically isolates the diffusion signal from the measurement noise. This technique fits the data spectrum using a parameterization of the signal and a least-squares method to optimize the fit of the parameterization to the data by varying four parameters. The parameterization P_s is the sum of two functions:

$$P_s = P_0 e^{-k^2\sigma^2} + \frac{\varsigma_\eta^2 \Delta}{\left|1 - a_1 \exp\left(-ik\Delta\right)\right|^2}, \tag{8}$$

where the varied parameters are a_1, the AR-1 coefficient; ς_η^2, the variance of the noise; and $\frac{1}{\Delta}$, the sampling frequency. The first function is a Gaussian, the exponential model representing the high-frequency damping of firn diffusion, and the second function is an autoregressive noise signal of order 1 (AR-1), representing noise added from the measurement process. The parameters are allowed to vary within bounds that are wide enough to not restrict the least-squares fit, but narrow enough to keep each function on the corresponding part of the curve.

This two-function technique has been used effectively to estimate diffusion lengths on many discretely-sampled data sets [*Gkinis et al.*, 2014; *Holme et al.*, 2017]. When applying this technique to CFA data sets, we find that the deviation from the exponential model in the CFA spectra affects the technique's ability to effectively fit the data. Figure 2 illustrates this issue with examples from the WDC and SPC ice cores. The poor total fit of the two-function model to the data spectrum results in a poor estimation of diffusion length.

Jones et al. [2017a] developed a method specifically for CFA data that avoids this issue. This technique identifies the frequency at which the spectrum deviates from the exponential model and only includes lower frequencies in the Gaussian fit. Figure 3 shows examples of this cut-off technique for data sections from WDC and SPC. This technique relies on the assumption that enough of the diffusion signal is preserved below the chosen cut-off frequency to result in a reliable diffusion estimate. This technique works well to avoid the issue of the deviation from the exponential model, but the technique is subjective

and tedious because it relies on determining cut-off frequencies by eye for each individual spectrum. A more objective and efficient technique that works with CFA data is needed.

5. Generalizing the Fitting Technique

We consider two different approaches to a general fitting technique that works for CFA data and can also be applied to discrete data. The first approach masks the CFA high-frequency deviation from the exponential model by adding white noise to the data so that the two-function technique can be applied. The second approach builds on the two-function technique by including a third function in the parameterization that accounts for the slower decay of the CFA power spectra. In the following section, each technique is introduced and illustrated on data sections from WDC and SPC.

5.1. Technique 1: Adding White Noise

In order to fit the CFA spectrum using the two-function technique described in Equation 8, this technique masks the slow decay of the spectrum by adding noise to the signal. We add normally-distributed noise in the time domain, which increases the noise level in the frequency domain. With this added noise, the resulting power spectrum is much closer to the exponential model, and the two-function technique of *Gkinis et al.* [2014] can now be effectively applied to the spectrum. Figure 4 illustrates this technique applied to a WDC data section. The disadvantage of this technique is that it manipulates the original signal; while the added noise masks the slow spectral decay, it may also mask useful climate information.

We used a sensitivity test to optimize the magnitude of noise to add to the data. Adding too little noise does not effectively mask the deviation from the exponential model, but

adding too much noise risks masking the climate signal. The test used a 500-year moving window throughout the WDC record. For each windowed section, 100 diffusion lengths were estimated by adding an increasing white noise baseline to the data in each window. A diffusion length was estimated for each tested noise level on each 500-year window. We defined the optimal noise level as that at which the diffusion length estimates stopped changing with increasing noise. This level can be found when the gradient of diffusion length with respect to added noise level approaches zero. Figure 5 shows how this gradient changes for both δ^{18}O and δD throughout the WDC core. The optimal noise level is selected for each age as the lowest noise level with a gradient of approximately zero. For WDC, we found that the optimal added noise is Gaussian-distributed noise with a standard deviation of 0.4 ‰ for δ^{18}O and 3.0 ‰ for δD.

5.2. Technique 2: Parameterizing a Multi-Function Fit

This technique creates a multi-function parameterization of the total spectrum by adding a third function to the two-function technique of *Gkinis et al.* [2014]. We tested three different functions by adding them each as a third term in Equation 8, and we determined which addition yields the best full-spectrum fit. The three functions we tested were a second AR-1 function, a second Gaussian function, and a folded normal distribution (FND) [*Tsagris et al.*, 2014]:

$$\phi = \phi_0 \cdot e^{-(k\cdot\psi)^2} \cdot |\,[1 - \Phi(-ik\psi)]\,|^2, \tag{9}$$

where $\Phi(\psi) = 1/2 \cdot \mathrm{erfc}(-\psi/2)$. Here ϕ_0 and ψ are the two parameters that are varied to optimize the fit. The justification of fitting a FND is that it reflects the unidirectional memory and diffusion induced by the one-way flow of the CFA system. A FND is the

absolute value of a Gaussian distribution, resulting in a function that smooths in only one direction. Because water is continuously flowing in one direction in the CFA system, the application of a FND mimics this one-sided effect.

The results of each of these three parameterizations for WDC and SPC are shown in Figures 6 through 8. Figure 6 shows the parameterization that sums a Gaussian curve and two autoregressive noise functions. With the inclusion of this third function in both WDC and SPC, the total fit is visually improved, as compared to the single-Gaussian fit in Figure 2, but still unable to effectively fit the spectrum, particularly for WDC. Figure 7 shows the parameterization that sums two Gaussian curves and one autoregressive noise function. Similarly, there is a visual improvement in the total fit as compared to the single-Gaussian fit, now in both SPC and WDC. Finally, Figure 8 shows the parameterization that sums one Gaussian, one autoregressive noise function, and a FND function. Due to the close relationship between a Gaussian and a FND function, the fits in Figures 7 and 8 are very similar.

6. Evaluating Fitting Techniques

To determine which fitting technique is best, we compared the effectiveness of each. First, we evaluated each technique based on how well each procedure could fit the data spectra. We calculated the adjusted coefficient of determination ($\bar{r}^2$) as a metric of goodness of fit with the data. The coefficient of determination (r^2) is calculated by comparing the variability of the estimation errors with the variability of the original values. The adjusted coefficient of determination ($\bar{r}^2$) takes into account the number of variable pa-

rameters (p) as follows [*Theil*, 1961]:

$$\bar{r}^2 = 1 - (1 - r^2)\frac{n-1}{n-p-1}, \tag{10}$$

where n is the sample size. We must use the $\bar{r}^2$ for this comparison because the techniques have different numbers of variable parameters (the noise-adding technique has five parameters, while the multi-function parameterizations each have six). Figure 9 plots the $\bar{r}^2$ values as a function of age for WDC. The $\bar{r}^2$ values of the double-Gaussian and FND parameterizations are indistinguishable, so we only include the double-Gaussian result. All the parameterizations provide good fits ($\bar{r}^2 > 0.9$) to the data, but the best fits are obtained with the double-Gaussian and FND parameterizations. For simplicity and computational efficiency, we prefer the double-Gaussian over the FND parameterization.

As a second means of evaluation, we compared the resulting diffusion length estimates for the double-Gaussian parameterization and noise-adding techniques. Figure 10 shows the diffusion length estimates from each technique plotted with respect to age through the entire WDC record. Both techniques reconstruct similar diffusion lengths, but the noise-adding method is more stable through the glacial period. This stability is attributed to the fact that, due to known measurement issues, the quality of some of the WDC data from the glacial period is poor. In this period, the water isotope signal contains several noisy sections of about half a meter, which produce spectra with strange characteristics. By adding white noise to the data, the noisy data sections are masked, making the fit more stable. Though, as discussed above, masking noisy sections of the data may also mask useful climate information. Besides this stability issue in the glacial period, the two techniques match well throughout the record, bolstering confidence in their fitting abilities.

NEED TO ADD SECOND GAUSSIAN TO FIG 10, OR ELSE REMOVE THIS PARAGRAPH: We can also study the stability of the multi-function technique by comparing how the added function varies through time. If the second Gaussian function is fitting a part of the spectrum that is determined by characteristics of memory in the CFA system, we expect that the standard deviation of that function should be relatively constant across all samples. Figure 10 also plots the corresponding diffusion length calculated from the standard deviation of the second Gaussian in the fit of each windowed section. The stability of the second Gaussian further supports the ability of this method to represent information about changing climate conditions in its fit of the diffusion Gaussian.

Another way of validating the results is by comparing with the diffusion lengths estimated with these techniques with those of the cut-off technique presented in *Jones et al.* [2017a]. Since these results are not affected by the deviation from the exponential model, we can use them as a benchmark against which to validate these new techniques. Figure 11 compares the two new techniques with the cut-off technique for the WDC record. The estimated diffusion lengths from this paper are very similar to those presented in *Jones et al.* [2017a], again adding confidence to the validation of our techniques. A few differences stand out in the comparison, such as the peaks around 12,000 and 14,000 years before present. These deviations are either due to differences in resolution of diffusion estimates or else due to differences in estimates of the power spectra.

7. Discussion

Through these evaluations, we conclude that the best technique for estimating diffusion length is the multi-function fit with the double-Gaussian parameterization, though the noise-adding method is also an option. While we have shown that these techniques can

be used to estimate the extent of firn diffusion, it remains unexplained why the spectra of continuously-measured data decay more slowly in the higher frequencies than the ideal exponential model. In this section we present some ideas about the cause of this spectral behavior.

There are many possible sources of noise throughout the CFA measurement system that could affect the spectrum. Mixing and memory effects are known to occur throughout the system as sample water travels to the instrument through tubing and various reservoirs [*Gkinis et al.*, 2011]. For WDC, *Jones et al.* [2017b] ran mock ice of constant isotopic compositions through the CFA system. This created a step-change in isotopic value and characterizes the response of the system to isotopic changes. [*Jones et al.*, 2017b] showed how this response can be estimated as a transfer function of the product of two lognormal CDFs:

$$\delta_{model}(t) = \frac{1}{2}\left[1 + erf\left(\frac{t-\mu_1}{\sigma_1\sqrt{2}}\right)\right] \cdot \frac{1}{2}\left[1 + erf\left(\frac{t-\mu_2}{\sigma_2\sqrt{2}}\right)\right] \tag{11}$$

Through forward modeling of synthetic ice core data, we found that WDC data spectra can be simulated by using a diffusion process following this function. We estimated the parameters of Equation 11 by minimizing the fit between the WDC data spectrum and the specrum of synthetic ice core data smoothed by this function. We checked this estimate by comparing the resulting transfer function with that calculated directly from the mock ice run through the CFA system. In this way, we found that the smoothing process can be explained by this forward smoothing process. Inverting this process to find a function to use in the above parametrization would be quite complicated. However, the FND function that we discuss in section 5.2 approximates the diffusion physics that occur.

We subsequently show that the double-Gaussian function gives indistinguishable results from the FND function, and thus the double-Gaussian parameterization can be used to approximate the complex behavior of the above transfer function.

While considering the CFA system response to isotopic changes characterizes the entire system, we can also think about the response to isotopic changes within distinct parts of the system. For example, a specific source of memory or mixing within the system is within the Picarro laser spectrometer. Within the instrument, the water vapor sample is input into a cavity where the isotopic composition is determined by measuring how quickly certain frequencies of a laser are absorbed by the sample. This measurement is affected by the amount of sample that remains in the cavity after most of it has been flushed out. Because there is a continuous stream of new sample vapor pumping into the cavity, the extent of this memory within the system will affect subsequent measurements. The timescales involved in this process can also explain the spectral behavior seen in the continuously-measured data.

The question as to the exact source of this slow decay of power in the continuously-measured data remains open, but these ideas give some insight into how the system is likely influencing the data spectrum.

8. Conclusions

In this study we examined the firn diffusion signal in continuously-measured water-isotope data from the WAIS Divide and South Pole ice cores. We observed that spectra from these CFA data, unlike spectra from comparable discretely-sampled data, have a different spectral behavior that deviates from the ideal exponential model. Previous diffusion-length estimate techniques fail to properly fit these CFA data due to this slower

decay of power. We found that the most effective way to estimate diffusion lengths on these CFA data is the double-Gaussian parameterization of the multi-function fitting technique, while the noise-adding technique can be used as well. These methods are efficient in required time and effort and also effective in fitting the entire spectra of continuously-measured data. We validated the method against one another as well as against diffusion lengths calculated independently by *Jones et al.* [2017a]. The exact cause of this spectral behavior within the CFA system remains an open question. However, these methods can be used to determine diffusion lengths on water isotope data from any ice core record of sufficiently high resolution and will be used in the future to investigate firn diffusion for the entire SPC record.

Acknowledgments. The research leading to these results was funded by the National Science Foundation grant numbers 1443105 and 1443328 as well as from the European Research Council under the European Union's Seventh Framework Programme (FP7/2007-2013) grant agreement #610055 as part of the ice2ice project.

References

Brand, W. A., Geilmann, H., Crosson, E. R., & Rella, C. W. (2009), Cavity ringdown spectroscopy versus hightemperature conversion isotope ratio mass spectrometry; a case study on 2H and 18O of pure water samples and alcohol/water mixtures, *Rapid Communications in Mass Spectrometry*, *23*(12), 1879–1884.

Casey, K. A., Fudge, T. J., Neumann, T. A., Steig, E. J., Cavitte, M. G. P., and Blankenship, D. D. (2014), The 1500 m South Pole ice core: recovering a 40 ka environmental record, *Annals of Glaciology*, *55*(68), 137–146.

Cuffey, Kurt M. and Eric J. Steig. (1998), Isotopic diffusion in polar firn: implications for interpretation of seasonal climate parameters in ice-core records, with emphasis on central Greenland, *Journal of Glaciology*, *44*.(147), 273–284.

Dansgaard, W. (1954), The ^{18}O-abundance in fresh water, *Geochimica et Cosmochimica Acta*, *6*(5-6), 241–260.

Dansgaard, W. (1964), Stable isotopes in precipitation, *Tellus B*, *16*(4), 436–468.

Dansgaard, W. and S. J. Johnsen (1969), A flow model and a time scale for the ice core from Camp Century, Greenland, *Journal of Glaciology*, *8*(53), 215–223.

Emanuelsson, B. D., Baisden, W. T., Bertler, N. A. N., Keller, E. D. and V. Gkinis (2015), High-resolution continuous-flow analysis setup for water isotopic measurement from ice cores using laser spectroscopy, *Atmospheric Measurement Techniques*, *8*(7), 2869–2883.

Epstein, S., Buchsbaum, R., Lowenstam, H. and H.C. Urey (1951), Carbonate-water isotopic temperature scale, *Geological Society of America Bulletin*, *62*(4), 417–426.

Gkinis, V., Popp, T. J., Blunier, T., Bigler, M., Schupbach, S., Kettner, E. and S. J. Johnsen (2011), Water isotopic ratios from a continuously melted ice core sample, *Atmospheric Measurement Techniques*, *4*(11), 2531–2542.

Gkinis, V. (2011), High resolution water isotope data from ice cores, PhD thesis, University of Copenhagen.

Gkinis, V., Simonsen, S. B., Buchardt, S. L., White, J. W. C. and B. M. Vinther (2014), Water isotope diffusion rates from the NorthGRIP ice core for the last 16,000 years - glaciological and paleoclimatic implications, *Earth and Planetary Science Letters*, *405*, 132–141.

Gupta, P., Noone, D., Galewsky, J., Sweeney, C., & Vaughn, B. H. (2009), Demonstration of highprecision continuous measurements of water vapor isotopologues in laboratory and remote field deployments using wavelengthscanned cavity ringdown spectroscopy (WSCRDS) technology, *Rapid Communications in Mass Spectrometry*, *23*(16), 2534–2542.

Herron, M., and Langway Jr, C. (1980). Firn densification: An empirical model. Journal of Glaciology, 25(93), 373-385.

Holme, C., Gkinis, V., and B. M. Vinther (2017), Molecular diffusion of stable water isotopes in polar firn as a proxy for past temperatures, Under review in *Geochimica et Cosmochimica Acta*.

Jones, T. R., Cuffey, K. M., White, J. W. C., Steig, E. J., Buizert, C., Markle, B. R., McConnell, J. R. and M. Sigl (2017a), Water isotope diffusion in the WAIS Divide ice core during the Holocene and last glacial, *J. Geophys. Res. Earth Surf.*, *122*, 290309.

Jones, T. R., White, J. W. C., Steig, E. J., Vaughn, B. H., Morris, V., Gkinis, V., Markle, B. R. and S. W. Schoenemann (2017b), Improved Methodologies for Continuous Flow Analysis of Stable Water Isotopes in Ice Cores, *Atmos. Meas. Tech. Discuss*, *10*, 617-632.

Johnsen, S. J. (1977), Stable Isotope Homogenization of Polar Firn and Ice, *Isotopes and Impurities in Snow and Ice*, 201–219.

Johnsen, S. J., Clausen, H. B., Cuffey, K. M., Hoffmann, G., Schwander, J. and T. Creyts (2000), Diffusion of stable isotopes in polar firn and ice: the isotope effect in firn diffusion, *Physics of Ice Core Records*, 121–140.

Kerstel, E. T., Van Trigt, R., Reuss, J., & Meijer, H. A. J. (1999), Simultaneous determination of the 2H/1H, 17O/16O, and 18O/16O isotope abundance ratios in water by

means of laser spectrometry, *Analytical Chemistry*, *71*(23), 5297–5303.

Lasaga, A. C. (2014), Kinetic theory in the earth sciences, *Princeton University Press*.

Lis, G., Wassenaar, L. I., & Hendry, M. J. (2008), High-precision laser spectroscopy D/H and 18O/16O measurements of microliter natural water samples, *Analytical Chemistry*, *80*(1), 287–293.

Oerter, H., Graf, W., Meyer, H. and F. Wilhelms (2004), The EPICA ice core Droning Maud Land: first results from stable-isotope measurements, *Ann. Glaciol.*, *39*, 307–312.

Simonsen, S. B., Johnsen, S. J., Popp, T. J., Vinther, B. M., Gkinis, V. and H. C. Steen-Larsen (2011), Past surface temperatures at the NorthGRIP drill site from the difference in firn diffusion of water isotopes, *Climate of the Past*, *7*, 1327–1335.

Steig, E. J., Ding, Q., White, J. W. C., Kttel, M., Rupper, S. B., Neumann, T. A., Neff, P. D., Gallant, A. J. E., Mayewski, P. A., Taylor, K. C., Hoffmann, G., Dixon, D. A., Schoenemann, S. Markle B. M., Schneider, D. P., Fudge, T. J., Schauer, A. J., Teel, R. P., Vaughn, B., Burgener, L., Williams, J. and E. Korotkikh (2013), Recent climate and ice-sheet change in West Antarctica compared to the past 2000 years, *Nature Geoscience*, *6*.

Steig, E. J., Gkinis, V., Schauer, A. J., Schoenemann, S. W., Samek, K., Hoffnalge, J., Dennis, K. J., and S. M. Tan. (2014), Calibrated high-precision 17 O-excess measurements using cavity ring-down spectroscopy with laser-current-tuned cavity resonance, *Atmospheric Measurement Techniques*, *7*(8), 2421–2435.

Svensson, A., Fujita, S., Bigler, M., Braun, M., Dallmayr, R., Gkinis, V., Goto-Azuma, K., Hirabayashi, M., Kawamura, K., Kipfstuhl, S., Kjr, H. A., Popp, T., Simonsen, M., Steffensen, J. P., Vallelonga, P. and Vinther, B. M. (2015), On the occurrence of annual

layers in Dome Fuji ice core early Holocene Ice, Climate of the Past, *11*, 1127–1137.

Theil, H. (1961), Economic Forecasts and Policy, *2nd Edition*, North-Holland, Amsterdam.

Tsagris, M., Beneki, C. and H. Hassani (2014), On the Folded Normal Distribution, *Mathematics*, *2*, 12–28.

van der Wel, G., Fischer, H., Oerter, H., Meyer, H. and H. A. J. Meijer (2015), Estimation and calibration of the water isotope differential diffusion length in ice core records, *The Cryosphere*, *9*(4), 1601–1616.

Whillans, I. M., and P. M. Grootes (1985), Isotopic diffusion in cold snow and firn, *J. Geophys. Res.*, *90*(D2), 3910–3918.

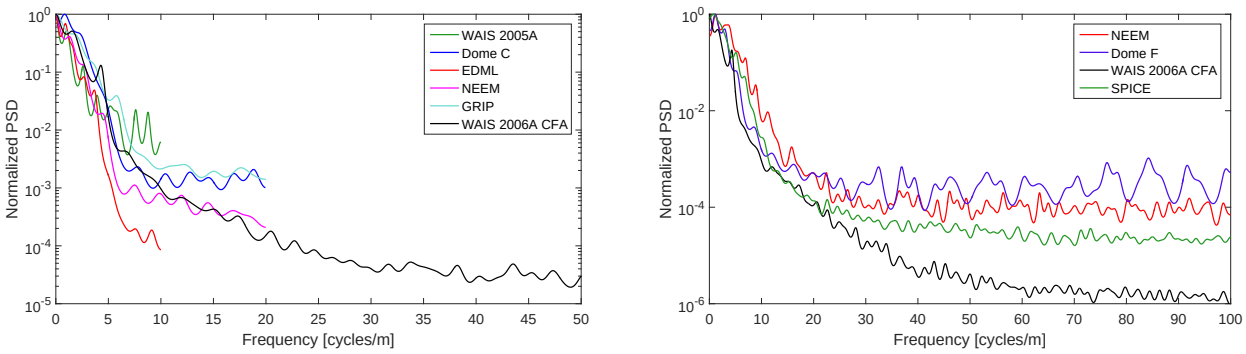

Figure 1: Left panel: The normalized PSD of five discretely measured δ^{18}O series plotted together with the PSD of a δ^{18}O WDC section. Right panel: The normalized PSD of four continuously measured δD series.

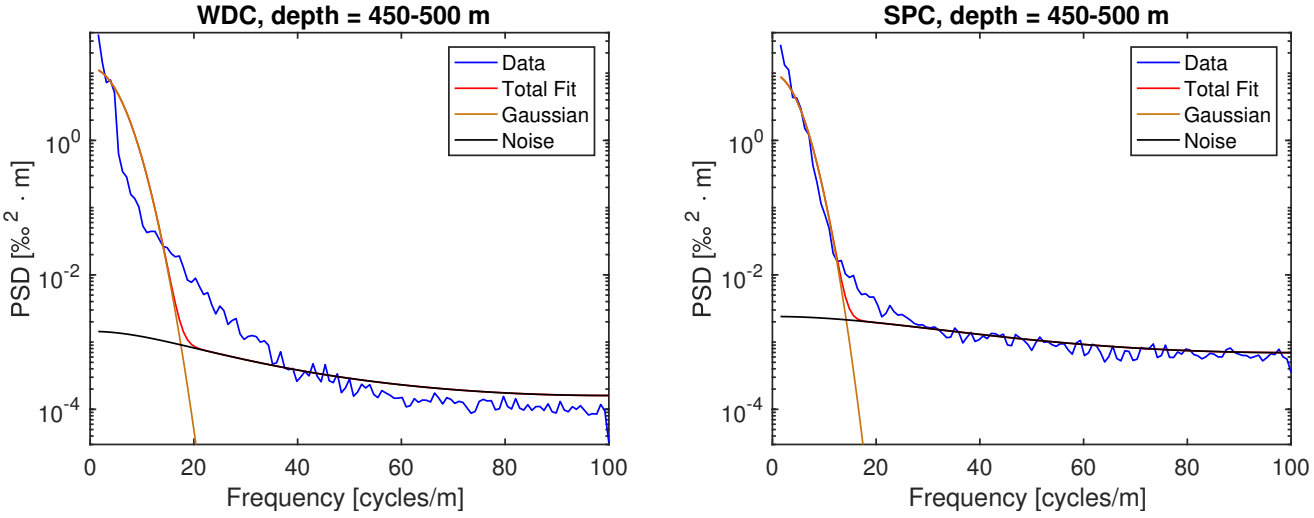

Figure 2: Single-Gaussian multi-function fits for WDC and SPC at 450-500m depth. With only two functions, the parameterization is unable to effectively fit the entire data spectrum.

Table 1: Summary of measurement specifications for each continuously measured core

Core	Picarro Instrument	Aquisition Rate	Melt Speed	Measurements Averaged
Dome F	1102	0.1 Hz	3 cm/min	∼1
NEEM	1102 (updated software)	0.2 Hz	3-4 cm/min	∼2
WDC	2130	1.2 Hz	2.5 cm/min	∼14
SPC	2140	1.2 Hz	2.25 cm/min	∼15

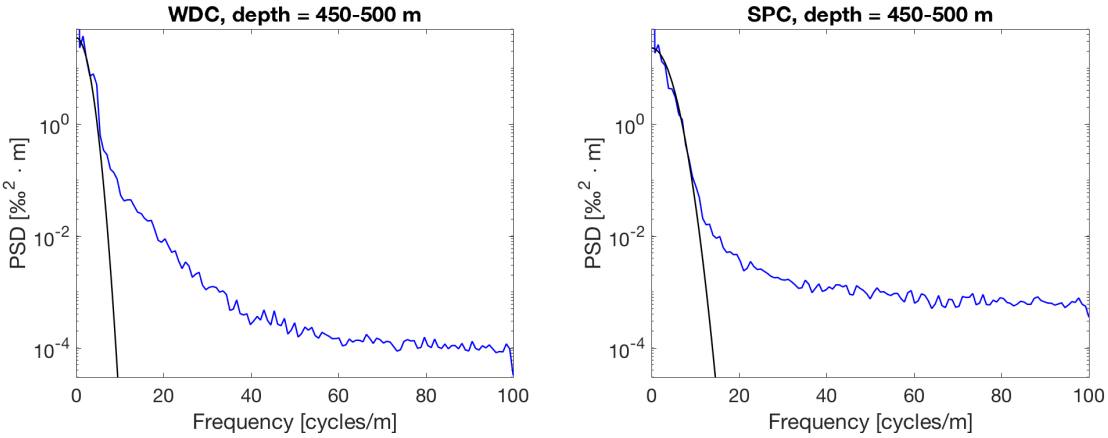

Figure 3: Cut-off technique on WDC and SPC at 450-500m depth. Blue curve is data spectrum and black curve is Gaussian fit.

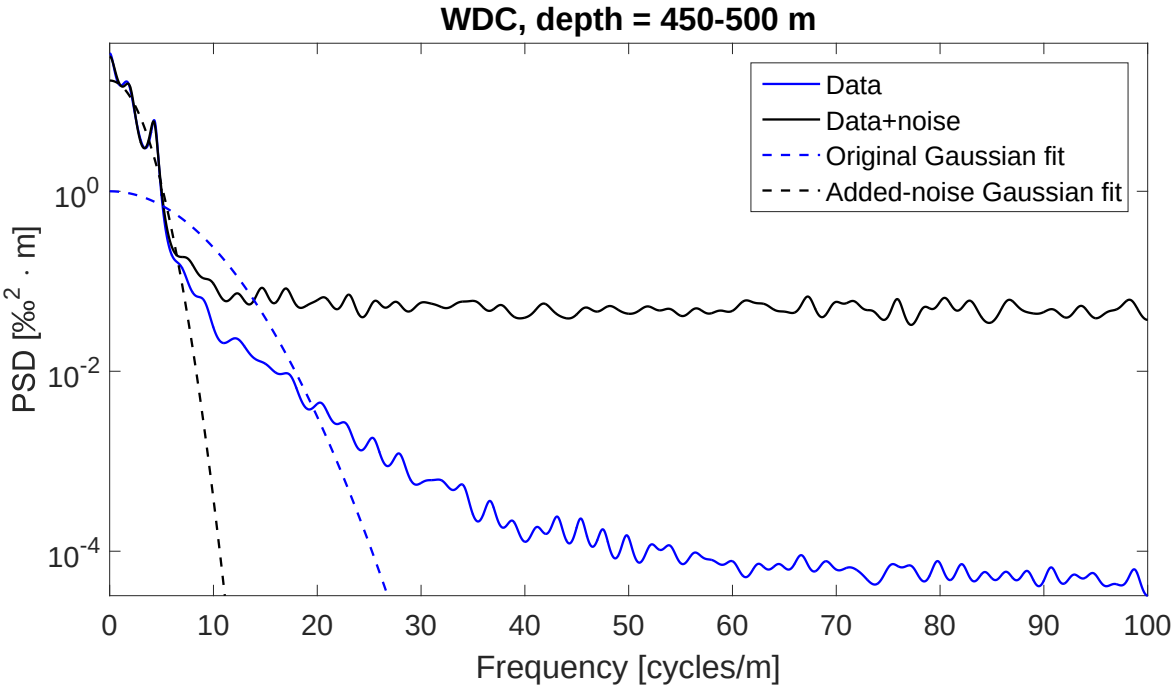

Figure 4: An illustration of the noise-adding technique for a δD section from WDC. The solid blue curve is the un-modified data and the black curve is data with noise added. The dashed lines represent the Gaussian functions fit using the two-function fitting technique. With the added noise, the dashed black model is able to effectively fit the data spectrum.

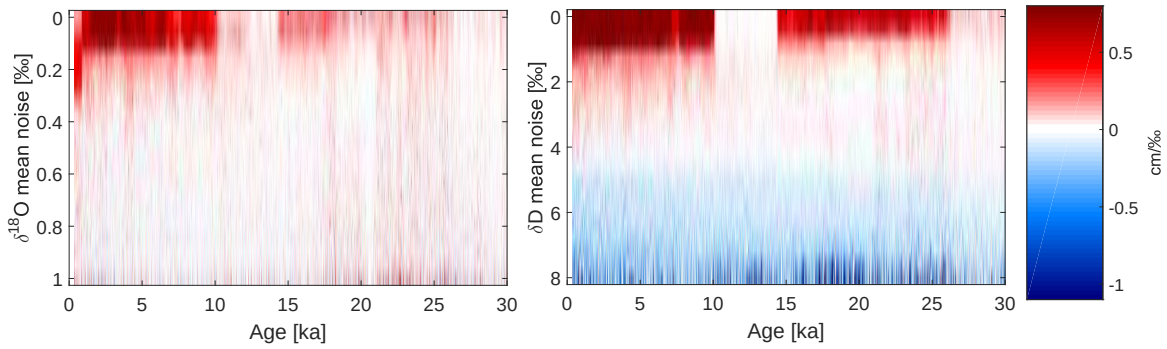

Figure 5: For WDC, the gradient of estimated diffusion lengths with respect to noise level plotted as a function of age. At each age, the lowest noise-level with a gradient of approximately zero is chosen as the optimal noise-level to be added.

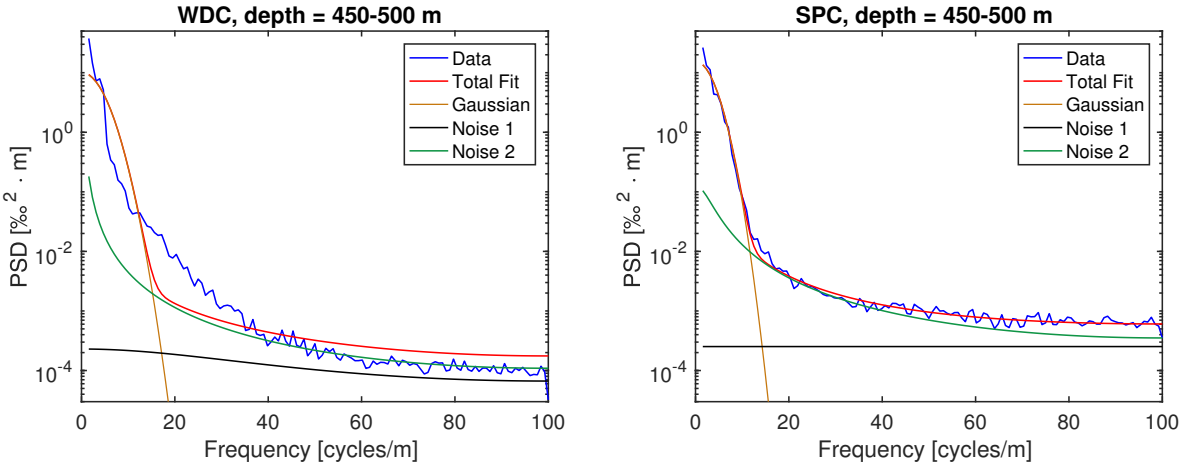

Figure 6: Single Gaussian and two autoregressive-noise functions fit to WDC and SPC spectra.

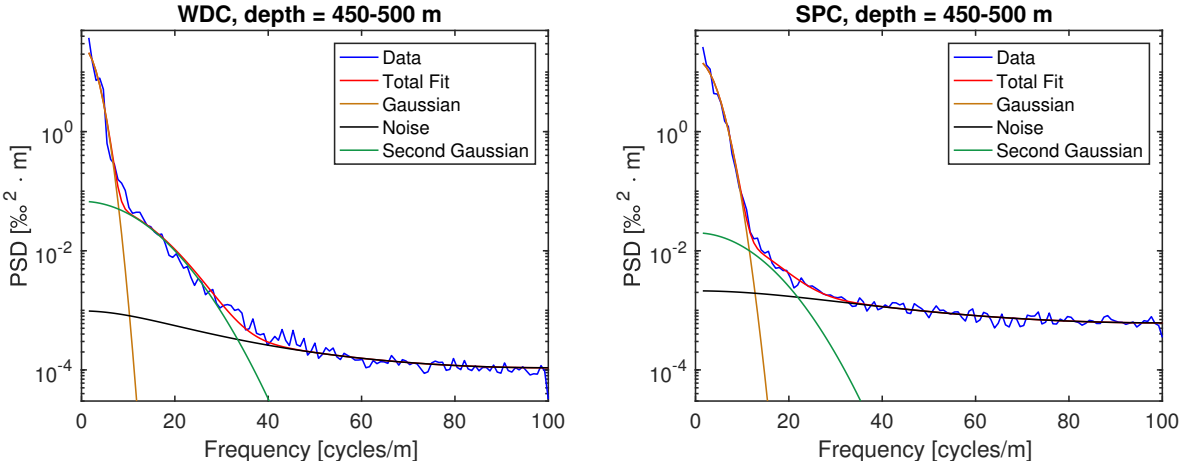

Figure 7: Double-Gaussian multi-function technique fit to WDC and SPC spectra.

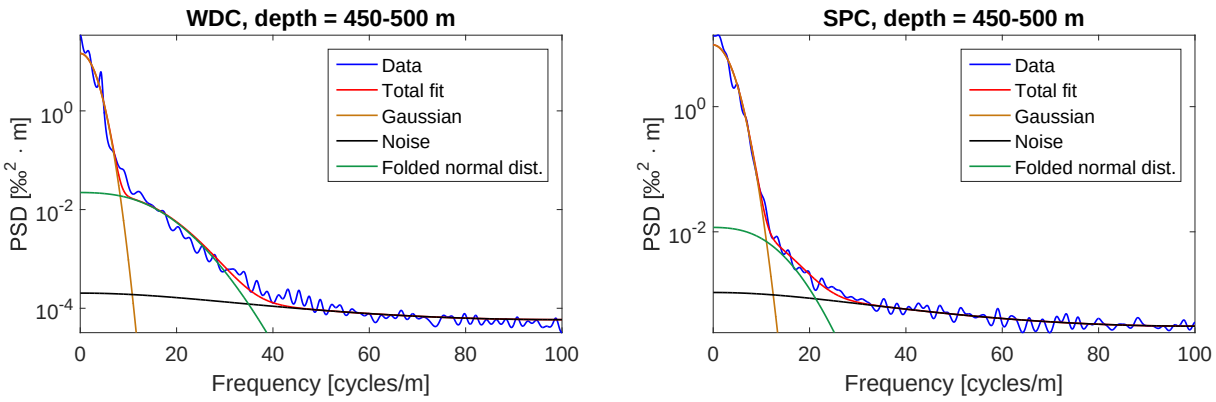

Figure 8: Folded normal distribution multi-function technique fit to WDC and SPC spectra.

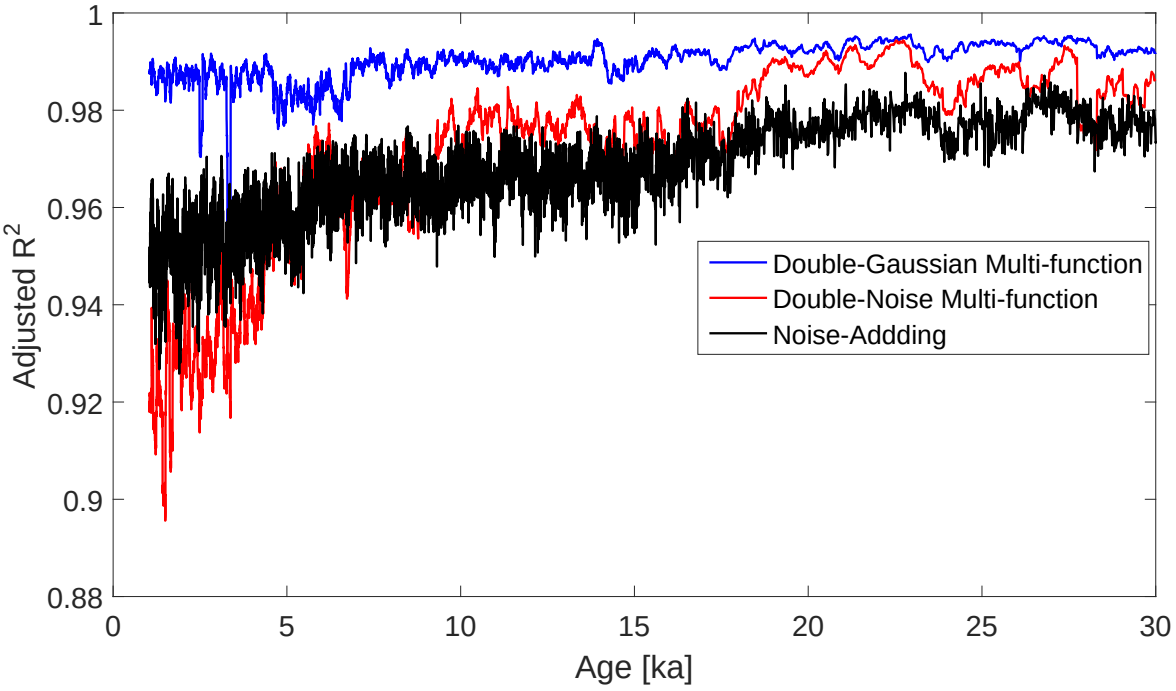

Figure 9: For WDC, the adjusted goodness of fit calculations through age for each fitting technique. FND results are identical to the results of a Gaussian curve and are not shown.

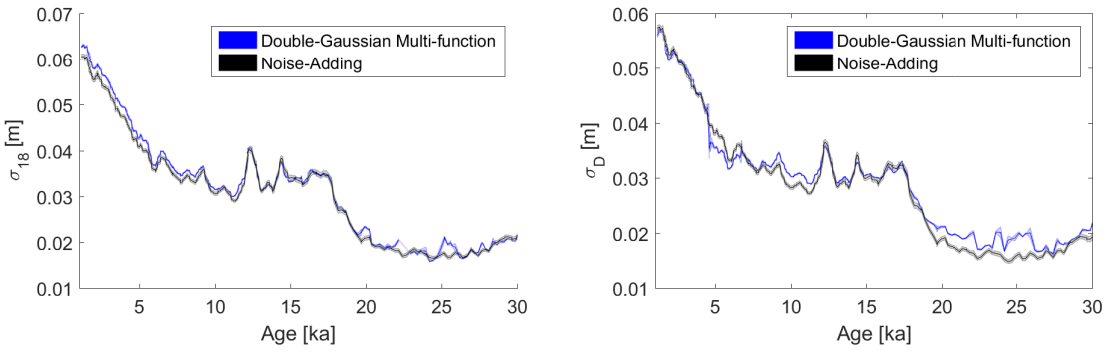

Figure 10: WDC diffusion lengths of δ^{18}O (left) and δD (right). Blue curve shows the multi-function Double-Gaussian technique, and the black curve shows the noise-adding technique.

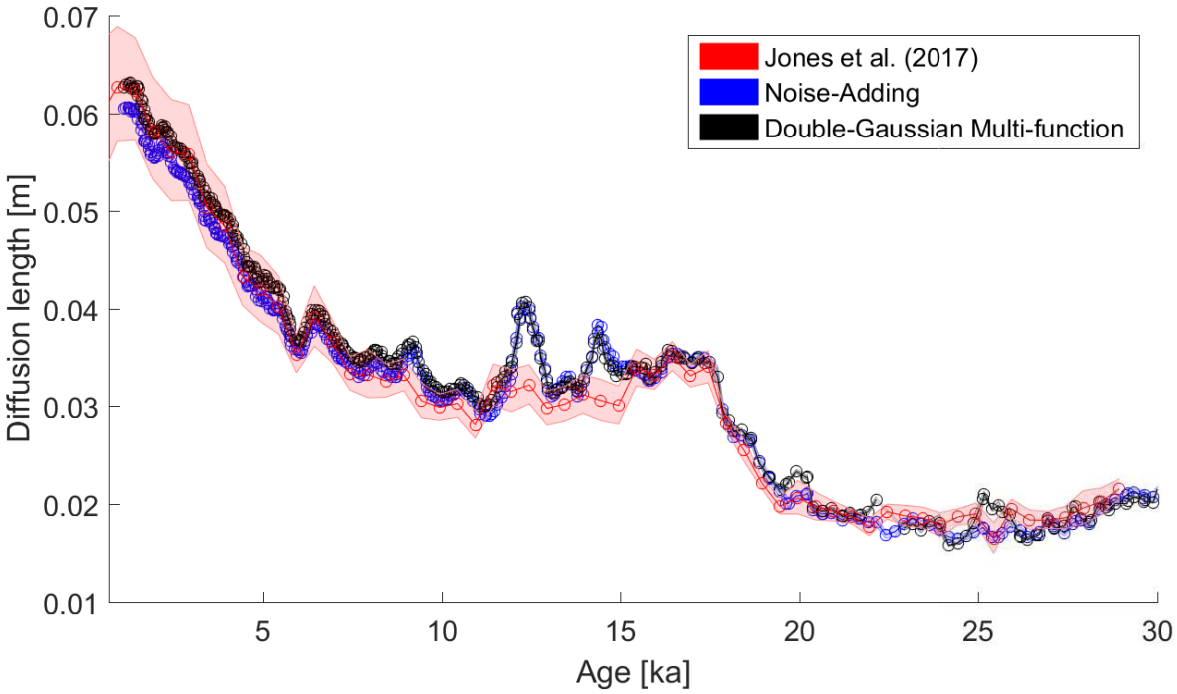

Figure 11: Estimated WDC diffusion lengths of δ^{18}O compared with those from *Jones et al.* [2017a].